CEBAF Program Advisory Committee Six (PAC6) Proposal Cover Sheet

This proposal must be received by close of business on April 5, 1993 at:

CEBAF

User Liaison Office

12000 Jefferson Avenue

Newport News, VA 23606

Proposal Title

Neutron Polarization Measurements in the $d(e, e'\vec{n})p$ Reaction Near Threshold

Contact Person

Name: R. Madey / A. Afasanev (Contact Person) Kharkov Institute, Kharkov

Institution: Kent State University/Hampton University/Kharkov Institute

Address:

Address: E-Mail: A. Afasanev: IN%"STERV%SPTC.KHARKOV.UA%RELAY.USSR.EU.NET"

City, State ZIP/Country: Kent, Ohio 44242 / Hampton, VA 23668 / Kharkov, 310108, Ukraine

Phone: (216)-672-2596 / (804)-727-5277 **FAX:**(216)-672-2959 / (804)-727-5188

E-Mail → BITnet: **Internet:** IN%"MADEY@KSUVXA.KENT.EDU" IN%"MADEY@CEBAF.GOV"

If this proposal is based on a previously submitted proposal or letter-of-intent, give the number, title and date:

CEBAF Use Only

Receipt Date: 4/5/93 Log Number Assigned: PR 93-040

By: gp

NEUTRON POLARIZATION MEASUREMENTS IN THE $d(e,e'\vec{n})p$ REACTION NEAR THRESHOLD

A. V. Afanasev (Spokesman)
Kharkov Institute of Physics and Technology, Kharkov 310108, Ukraine
R. Madey (Co-Spokesman), B. D. Anderson, A. R. Baldwin, T. Eden, D. Keane, A. Lai, D. M. Manley, J. W. Watson (Co-Spokesman), W.-M. Zhang
Kent State University, Kent, OH 44242
S. Nanda, A. Saha, P. E. Ulmer
CEBAF, Newport News, VA 23606
K. Baker, K. B. Beard, S. Beedoe, W. W. Buck, L. Tang
Hampton University, Hampton, VA 23668
J. M. Finn
College of William and Mary, Williamsburg, VA 23185
R. Lourie
University of Virginia, Charlottesville, VA 22904
P. J. Pella
Gettysburg College, Gettysburg, PA 17325
B. Flanders
American University, Washington, D.C. 20016
C. Howell, W. Ternow, R. Walter
Duke University, Durham, NC 27707

April 5, 1993

[This document was prepared by A. Afanasev, R. Madey, and T. Eden]

Abstract

We propose to measure the final neutron polarization in the $d(e,e'\vec{n})p$ reaction near threshold for transferred momenta $0.6 \leq Q^2(\mathrm{GeV/c})^2 \leq 1.2$. We argue in favor of studying a normal component of the neutron polarization vector for electron scattering at small angles, where the cross sections are large. These measurements would provide independent information about the magnitude and sign of the $M1 \rightarrow {}^1S_0$ transition amplitude which is affected strongly by nonnucleonic degrees of freedom in the deuteron.

1 Introduction

Measurements of deuteron electrodisintegration cross sections near threshold for large electron scattering angles and high momentum transfers [1-3] provided convincing evidence for nonnucleonic degrees of freedom in the deuteron. In order to reconcile theoretical concepts of the deuteron to these measurements, it has been shown that nonnucleonic degrees of freedom and meson exchange currents (MEC) in particular should be considered[4]; and at $Q^2 > 1.0$ $(\mathrm{GeV}/c)^2$, isobaric configurations [4], heavy meson exchanges [5], and quark degrees of freedom [6] can be significant also.

Generally, most of the theoretical models are unable to give a consistent description of the data [1-3] along with SLAC measurements [2] at higher $Q^2 < 2.77$ $(\mathrm{GeV}/c)^2$. Also, in recent MIT/Bates data with higher accuracy [3] at $Q^2 < 49$ fm^{-2}, a diffractive minimum of the cross section vs. Q^2 was not observed, though predicted by a number of models; however, in some models the diffractive minimum does not show up basically because they include other multipoles in addition to the $M1 \rightarrow {}^1S_0$ transition, and they differ at large Q^2 because of subtle features of the models. The cross section measurements to be done at CEBAF [7] will cover the range of Q^2 up to 3.5 $(\mathrm{GeV/c})^2$ which will put rigorous constraints on theoretical models of the processes in the nucleus at short distances.

In addition to obtaining data to resolve the above discrepancies, it would be desirable to study the spin and the isospin structure of the threshold transition $\gamma^* d \rightarrow np$ (γ^* being a virtual photon). As was shown earlier by Afanasev and Rekalo [8, 9], this information can be retrieved from polarization experiments. For the kinematic domain being considered here, final neutron polarization measurements offer an opportunity to obtain the desired information. In this proposal, we demonstrate that measurements of the recoil neutron polarization in the $d(e,e'\vec{n})p$ reaction yields information about the absolute values and the relative phase of the $M1$ and the $E0$, isovector and isoscalar, multipole transition form factors near threshold. This polarization can be studied at small electron scattering angles where the cross sections are large. There is a unique opportunity at CEBAF to investigate the neutron polarization in the threshold $d(e,e'\vec{n})p$ reaction in the most interesting kinematic regime (for the physics of nonnucleonic degrees of freedom in the deuteron) around $Q^2 \simeq 1.0$ $(\mathrm{GeV}/c)^2$.

In Section 2, we outline a general formalism for polarization observables, introduce definitions of threshold electromagnetic form factors, and present different components of the neutron polarization vector in the $d(e,e'\vec{n})p$ reaction in terms of these threshold electromagnetic form factors. In Section 3, predictions of a relativistic model are given. In Section 4, an experimental arrangement is described; and count rate estimates are given in Section 5 for specific experimental conditions.

2 Formalism for Polarization Observables and Threshold Electromagnetic Form Factors

For the scattering of longitudinally–polarized electrons with polarization h, the final nucleon polarization vector can be defined in terms of nine structure functions, which in turn can be expressed as bilinear combinations of eighteen independent scalar (or helicity) complex amplitudes of the $\gamma^* d \to np$ process [10]. Near threshold, the final nucleons are emitted basically along the direction of the transferred momentum; in addition, dominant amplitudes of transitions into S-waves of the final nucleons exhibit no angular dependence (in c.m.s.) For these reasons, it is sufficient and more convenient to study the observables integrated over the solid angle of the final nucleon . In this case, the final neutron polarization vector is determined as [8]

$$\begin{aligned} \mathbf{P}\frac{d^2\sigma}{dE'd\Omega_e} &= N\Big[\mathbf{x}h\sqrt{\epsilon(1-\epsilon)}P_{1n} + \mathbf{y}\sqrt{\epsilon(1+\epsilon)}P_{2n} \\ &\quad + \mathbf{z}h\sqrt{1-\epsilon^2}P_{3n}\Big], \\ N &= \frac{\alpha^2}{16\pi^2}\frac{E'}{E}\frac{|\mathbf{p}|}{MW}\frac{1}{(1-\epsilon)(-k^2)} \end{aligned} \tag{1}$$

while the differential cross section is given by

$$\frac{d^2\sigma}{dE'd\Omega_e} = N[\sigma_T + \epsilon\sigma_L] \tag{2}$$

where k is a transferred four–momentum, $Q^2 = -k^2$, $\epsilon^{-1} = 1 - \frac{\mathbf{k}^{lab}}{k^2}\tan^2\frac{\theta_e}{2}$, $E(E')$ is an initial (final) electron energy, θ_e is an electron scattering angle, M is a deuteron mass, W is a total energy of the n–p system, $-\mathbf{p}$ is a neutron three-momentum transfer in the c.m.s., and k^{lab} is the three–momentum of the neutron in the lab system. The coordinate system is chosen as follows: $\mathbf{z} = \frac{\mathbf{k}}{|\mathbf{k}|}$, $\mathbf{y} = \frac{\mathbf{k}\times\mathbf{k}_1}{|\mathbf{k}\times\mathbf{k}_1|}$, $\mathbf{x} = \mathbf{y}\times\mathbf{z}$, $\mathbf{k}_1$ being an initial electron momentum. The quantities P_{1-3}, σ_T, σ_L are functions of two kinematic variables, k^2 and W. The formulae (1) and (2) are general and assume only the validity of the one-photon exchange mechanism for e–d scattering and gauge invariance of the electromagnetic interaction.

Let us take advantage of the fact that only S-waves of the final n–p system predominate near the reaction threshold. Omitting other partial waves, we determine the amplitude $\mathcal{M}$ of the process $\gamma^* d \to np$ by five scalar functions or electromagnetic form factors (EFF) g_i, which account for its spin structure. Then the amplitude $\mathcal{M}$ reads (in c.m.s.) [11, 8]

$$\begin{aligned} \mathcal{M} &= e\varphi_1^+ F\sigma_2\tilde{\varphi}_2^+, \\ F &= ig_1\mathbf{eU}\times\hat{\mathbf{k}} + g_2\sigma\hat{\mathbf{k}}\cdot\mathbf{eU} + g_3\sigma\mathbf{e}\cdot\mathbf{U}\hat{\mathbf{k}} + \\ &\quad g_4\mathbf{e}\hat{\mathbf{k}}\cdot\sigma\hat{\mathbf{k}}\cdot\mathbf{U}\hat{\mathbf{k}} + g_5\mathbf{e}\hat{\mathbf{k}}\cdot\sigma\mathbf{U}, \end{aligned} \tag{3}$$

where $\varphi_1(\varphi_2)$ is a proton (neutron) spinor, $\mathbf{U}(\mathbf{e})$ is a three-vector of the deuteron (virtual photon) polarization and $\hat{\mathbf{k}}$ is a unit vector along the photon three-momentum. The EFF g_i in eq.(3) define absorption of the virtual photon γ^* with a certain multipolarity, viz., $M1 \to {}^1S_0(g_1)$ being an isovector transition, $M1 \to {}^3S_1$ $(g_2 - g_3)$, $E2 \to {}^3S_1$ $(g_2 + g_3)$, $E2_L \to {}^3S_1$ $(g_2 + g_3 + g_4)$, $E0_L \to {}^3S_1(g_5)$ being isoscalar transitions.

Equation (3) is exact at threshold where the energy of final nucleon relative motion $E_{np}^{c.m.} = 0$; in this case, the EFF g_i are real functions of k^2. If $E_{np}^{c.m.} \neq 0$, the EFF acquire phases that can be determined strictly on the basis of elastic unitarity and T-invariance of the scattering matrix

$$\begin{aligned} Im\ g_1 &= \tan\delta_s\ Re\ g_1, \\ Im\ g_{2-5} &= \tan\delta_t\ Re\ g_{2-5}, \end{aligned} \tag{4}$$

where $\delta_s(\delta_t)$ is the n–p scattering phase in the ${}^1S_0({}^3S_1)$ state.

Any polarization observables at threshold of $e^- + d \to e^- + n + p$ can be expressed in terms of EFF g_i. Thus we have for the neutron polarization structure functions,

$$\begin{aligned} P_{1n} &= \frac{4\sqrt{-2k^2}}{3k_0} Re[-(-g_1+g_2)g_5^* + \frac{\omega^2}{M^2} g_3(g_2+g_3+g_4+g_5)^*], \\ P_{2n} &= -\frac{4\sqrt{-2k^2}}{3k_0} Im(g_1 g_5^*), \\ P_{3n} &= \frac{4}{3} Re(-2g_1 g_2^* + \frac{\omega^2}{M^2}|g_3|^2), \end{aligned} \tag{5}$$

ω being the deuteron energy in the c.m.s. The cross section structure functions read in terms of g_i

$$\begin{aligned} \sigma_T &= \frac{4}{3}(|g_1|^2 + |g_2|^2 + |g_3|^2 \frac{\omega^2}{M^2}, \\ \sigma_L &= \frac{-4k^2}{3k_0^2}(|g_2+g_3+g_4+g_5|^2 \frac{\omega^2}{M^2} + 2|g_5|^2). \end{aligned} \tag{6}$$

Note in passing that P_x, $P_y = 0$ at $\theta_e = 0$ and 180 deg, and $P_z = 0$ at $\theta_e = 0$. The normal polarization component P_y is nonzero only if the EFF g_i have different phases. It follows from Eqs (4) and (5) that $P_y \propto \sin(\delta_s - \delta_t)$; i.e., P_y is caused by the difference between singlet and triplet phase shifts.

Expressions for the final proton polarization can be derived from Eq. (5) by changing the sign of g_1.

3 Numerical Estimates and Discussion

In order to make numerical estimates, we use a relativistic impulse approximation (RIA) [12] with FSI taken into account within a dispersion relation technique [8]. In this approximation, the scattering amplitude is described by a sum of three pole diagrams (with exchange of nucleons and a deuteron) and a contact diagram needed to ensure electromagnetic current conservation. "Pair currents" are incorporated consistently through negative–energy states of the deuteron wave function (DWF). As shown in Fig. 1, a particular choice of the DWF (and the $\gamma^* NN$ vertex) agrees well with the data [1-3] on the $d(e,e')pn$ cross section at both lower and higher Q^2 and reproduces the observed change of slope [3] around $Q^2 \approx 1.0$ (GeV/c)^2. This result means that negative–energy states of the DWF treated within a quasipotential approach [13] give rise to the similar effect as compared to "pair currents" in nonrelativistic approaches [4]. The contribution of negative–energy states increases with the parameter λ of the Buck-Gross DWF [13] and is maximal for pure pseudoscalar πNN–coupling (λ =1); however, note that this result may change when contact terms will

be included for the pseudovector part of πNN-coupling. The corresponding theoretical study is currently underway by one of us (A. Afanasev).

If we set to zero all the multipole amplitudes except the $M1 \to {}^1S_0$ amplitude, then as shown in Fig. 2, the cross section vs. Q^2 will have a dip around $Q^2 = 1.0$ (GeV/c)^2 where this amplitude changes its sign. The position of the zero of the $M1 \to {}^1S_0$ amplitude is very sensitive to theoretical models of non-nucleonic degrees of freedom in the deuteron. Unfortunately, this dip cannot be observed experimentally by measuring cross sections in the $d(e,e')pn$ reaction because the dip region is filled with contributions from other multipoles resulting at most in a change of slope; however, this dip can be observed in polarization experiments, as we will show below.

Let us analyze the model predictions for the polarization vector components of the neutron emitted in the reaction $e^- + d \to e^- + p + n$. We estimated all the three polarization components, P_x, P_y, and P_z at $E_{np}^{c.m.} = 1.5$ MeV. These quantities vs. Q^2 are affected by the following features of threshold amplitudes: a) a change of the G_1 sign at $Q^2 \approx 1.0$ (GeV/c)^2 as a result of destructive interference of transitions from the ${}^3S_1 + {}^3D_1 + {}^3P_1 + {}^1P_1$ deuteron bound states into the ${}^1S_0$ state of a continuous spectrum, and b) a change of the g_5 sign from the fact that near the threshold the sign is determined basically by an elastic deuteron EFF G_1 which changes its sign at $Q^2 = 0.45$ (GeV/c)^2 in the model used for the elastic deuteron EFF (with a pseudovector πNN coupling) [14].

For backward electron scattering, only the longitudinal proton polarization P_z "survives;" however, for these scattering angles and for the particularly interesting range of transferred momenta $Q^2 > 1.0$ (GeV/c)^2, the cross section is essentially suppressed making the measurements of P practically impossible to do because of low counting rates.

For forward electron scattering, there is no suppression of the differential cross section because of the longitudinal photon contribution; for example, at $Q^2 = 1.0$ (GeV/c)^2, the threshold cross section at $\theta_e = 20°$ is almost three orders-of-magnitude higher than the corresponding cross section at $\theta_e = 180°$ and at the same Q^2. For forward electron scattering, the components P_x and P_z are essentially suppressed, and P_y is the largest; moreover, P_y is determined directly from the product of the small EFF g_1 and the large EFF g_5 thus allowing a straightforward and independent measurement of the $M1 \to {}^1S_0$ transition amplitude (i.e., EFF g_1). In this respect, it would be of particular interest to find a Q^2 region where g_1 changes its sign. The normal component of the neutron polarization P_y is plotted in Fig. 3 as a function of Q^2. The situation is similar to the P_x polarization of the proton in the elastic e-p scattering determined by a (large) magnetic form factor G_M^p times a (small) electric form factor G_E^p making it possible to extract more accurate information on G_E^p as compared to the Rosenbluth separation technique.

It should be noted especially that P_y is an induced polarization that does not require a polarized electron beam.

4 Experimental Arrangement

Figure 4 is a schematic diagram of the experimental arrangement. An unpolarized electron beam is incident on an unpolarized liquid-deuterium target. A neutron polarimeter measures the normal polarization component P_y of the neutron at a laboratory emission angle θ_n. The High Resolution Spectrometer (HRS) measures the momentum of the electron scattered at an angle θ_e. The recoil neutron is measured in coincidence with the scattered electron. The neutron kinetic energy for real e-n coincidence events is obtained from a measurement of the neutron flight-time from the target

to the front analyzer detector in the neutron polarimeter.

4.1 Neutron Polarimeter

The neutron polarimeter shown in Fig. 5 was designed and constructed at Kent State University specifically for the measurement of the neutron electric form factor.[15] This polarimeter was calibrated in (August 1989) with polarized neutrons of about 135 MeV from the Indiana University Cyclotron Facility (IUCF).[16] This polarimeter consists of twelve 10.16 cm thick scintillation counters — four primary scatterers (1 through 4) and two sets of four rear detectors (5 through 12). The rear detectors are located at a polar angle θ with respect to the direction of the three–momentum transfer $\vec{q}$. For neutrons of about 135 MeV, $\theta \sim 21°$. The mean flight path from the point midway between primary scatterers #2 and #3 to the midpoint of each rear detector array is 2.0 m. All 12 scintillation detectors are mounted with the long dimension in the vertical direction. The rear scintillators are 1.016 m high by 0.508 m wide (NE–102) plastic; for this experiment, the front scintillators are 0.508 m high by 0.508 m wide (NE–102) plastic. In front of each set of four detectors, is a thin (0.95 cm) plastic scintillation counter to veto charged particles. The design of the polarimeter is based on properties of n–p scattering as a polarization analyzer. This polarimeter configuration (of four front analyzer scintillators and eight rear detectors for scattered neutrons) requires that the front and rear detector signals be processed independently to allow for simplified data processing and easy on–line observation of the relevant polarimeter signals.

4.2 Steel-Collimator and Shielding

Based on measurements of neutrons in the test runs at Bates (in February and June 1989), the neutron polarimeter must be contained in a shielding enclosure similar to that described below and in the proposal revision for CEBAF E89–05. In Bates E85–05, the rear wall and the two side walls are high density ($\rho = 3.9$ g/cm^3) concrete, four-feet thick, obtained from the Cambridge Electron Accelerator. The roof of the enclosure was covered with high–density concrete roof beams, two-feet thick. The interaction mean free path in normal density ($\rho = 2.3$ g/cm^3) concrete for 75 MeV neutrons is about one foot; therefore, the transmission of 75 MeV neutrons is about 1.8% through four feet; for high–density ($\rho = 3.9$ g/cm^3) concrete, the interaction mean free path is about 18 cm ($\sim$ 7 in) for 75 MeV neutrons and the transmission is about 0.10%. The front wall consists of lead, 4 in. thick, supported by two steel plates, each $1\frac{1}{4}$ in. thick; in addition, steel blocks were used to collimate the front detectors of the polarimeter and to provide additional shielding for the rear detectors. The transmission of neutrons with kinetic energies $\geq$ 100 MeV through this front shielding wall of 10.16 cm of lead plus 6.350 cm of steel is 39 percent. Because this front shielding wall contains about 22 radiation lengths, the reduction in energy of a high–energy photon incident on this front shielding is expected to be so large as to be below the detection threshold. A steel shadow shield, three–feet thick, was used to block the direct path of neutrons from the target to measure the room background. For this experiment, the inside dimensions of the shielding enclosure are 14 ft high by 9 ft wide by 14.2 ft long because the polarimeter here is rotated 90° (to measure P_y) with respect to that for the G_E^n measurement (to measure $P_{S'}$).

For CEBAF E89–05, we show the plan view of the shielding enclosure of the neutron polarimeter in Fig. 6; a side view was shown in Fig. 7. The rear wall and the two side walls are normal density ($\rho = 2.5$ g/cm^3) concrete, eight-feet thick, obtained from the University of Illinois accelerator. The

roof of the enclosure is covered with normal-density concrete roof beams, 42-inches thick. The front wall consists of lead, 4 in. thick, poured into steel containers with 1.25 in. walls. The shielding enclosure for CEBAF E89-05 together with the supporting base weighs about 1400 tons as listed below:

Shielding Components	Weights (tons)	
1. Shielding Enclosure		**530.4**
1.1 Sides (2.5 g/cm^3 concrete)	400.4	
1.2 Roof (2.5 g/cm^3 concrete)	126.5	
1.3 Floor (steel)	3.5	
2. Collimator		**120.4**
2.1 Steel (7.87 g/cm^3)	83.9	
2.2 Concrete (2.5 g/cm^3)	36.5	
3. Lead-steel Wall		**21.3**
4. Base (3.25 g/cm^3 concrete) No concrete below steel wall		**707.0**
TOTAL		**1379.1**

4.3 Solid-Angle Matching for Electron-Neutron Coincidences; Acceptances and Solid Angles

In order to optimize the electron–neutron coincidence rate, we want to provide the best match between the angular acceptance of the electron spectrometer and the angular acceptance of the neutron polarimeter; thus, we examine the matching in the horizontal (θ) and the vertical (ϕ^v) planes.

4.3.1 Horizontal (θ) Matching

For the case of deuteron electrodisintegration when $E_{np}^{c.m.} = 0$, transverse–momentum conservation ($p_\perp^e = p_\perp^{n+p}$) in the electron scattering plane requires that

$$p_\perp^e \equiv p_e \sin\theta_e = p_\perp^{n+p} = 2p_n \sin\theta_n \ . \tag{7}$$

Longitudinal–momentum conservation in the reaction plane requires

$$p_o = p_{||}^e + p_{||}^{n+p} = p_e \cos\theta_e + 2p_n \cos\theta_n \ . \tag{8}$$

Here the momentum of the incident electron $p_o = E$ in the approximation $m_e = 0$ (which we will use throughout this section), the momentum of the scattered electron $p_e = E' = E'(\theta_e)$, and p_n

is the momentum of the emitted neutron. These momentum conservation equations lead to the following kinematic relation:

$$\tan\theta_n = \left[\frac{W^2 - M^2}{2ME}\right]\left[\left(1 + \frac{E}{M}\right)\tan(\theta_e/2) + \frac{1}{\tan\theta_e}\frac{W^2 - M^2}{2ME}\right]^{-1} , \tag{9}$$

which implies the following expression for the derivative $(d\theta_n/d\theta_e)^k_E$:

$$\left(\frac{d\theta_n}{d\theta_e}\right)^k_E = -\sin^2\theta_n\left[\frac{1 + E/M}{2\cos^2(\theta_e/2)} - \frac{W^2 - M^2}{2ME}\frac{1}{\sin^2\theta_e}\right]\left[1 - \frac{W^2 - M^2}{2ME}\right]^{-1} . \tag{10}$$

Here the subscript E in $(d\theta_n/d\theta_e)^k_E$ denotes fixed E. The superscript k denotes that these expressions arise from kinematics. In this experiment the horizontal angular acceptance of the electron arm is fixed, *viz.*, $\Delta\theta_e = \pm\ 1.70°$ with the Hall A high–resolution spectrometer (HRS) in the normal operating mode; therefore, the kinematically–matched horizontal angular spread of the neutron flux can be calculated:

$$(\Delta\theta_n)^k_E = \left(\frac{d\theta_n}{d\theta_e}\right)^k_E \Delta\theta_e \ . \tag{11}$$

The results are given in Table I for a neutron flight path $x = 2.54$ m.

4.3.2 Vertical (ϕ^v) Matching

For electron scattering planes that are rotated about the beam axis through a small azimuthal angle ϕ with respect to the horizontal (reference) plane, the sum of the momentum components perpendicular to the horizontal plane must vanish; that is, at $E^{c.m.}_{np} = 0$ for electrodisintegration,

$$p^e_\perp \sin\phi_e = p^{n+p}_\perp \sin\phi_n \ , \tag{12}$$

or, in view of Eq. (7),

$$p_{e'} \sin\theta_e \sin\phi_e = 2p_n \sin\theta_n \sin\phi_n \ . \tag{13}$$

In this experiment, the vertical angular acceptance $\Delta\phi^v$ in the neutron arm is fixed with a given flight path x and a vertical dimension $h(= 0.508$ m) of the front detector in the neutron polarimeter; therefore, the vertical angular acceptance $\Delta\phi^v$ in the electron arm has to be matched to that of the neutron arm.

For the neutron arm,

$$\Delta\phi^v = \Delta\phi_n \sin\theta_n = \frac{h}{2x} \ , \tag{14}$$

and

$$\Delta\phi_n = \frac{\Delta\phi^v}{\sin\theta_n} = \frac{h}{2x\sin\theta_n} \ , \tag{15}$$

where θ_n is the neutron scattering angle. For $h = 0.508$ m, and $x = 2.54$ m, values of $\Delta\phi_n$ are listed in Table I for each Q^2 point. Because $\phi_e = \pi - \phi_n$, the magnitudes of the azimuthal angular intervals for electrons and neutrons are equal:

$$\Delta\phi_e = |\Delta\phi_n| \ . \tag{16}$$

Hence, this equality means that

$$\Delta\phi_e^{\rm v} = \Delta\phi_e \sin\theta_e = |\Delta\phi_n| \sin\theta_e = \frac{h}{2x}\frac{\sin\theta_e}{\sin\theta_n} = \frac{h}{2x}\frac{2p_n}{p_e} \quad . \tag{17}$$

The values of $\Delta\phi_e^{\rm v}$ are listed also in Table I.

Finally, the solid angle $\Delta\Omega$ is:

$$\Delta\Omega = 4\Delta\theta\Delta\phi\sin\theta = 4\Delta\theta\Delta\phi^{\rm v} \quad , \tag{18}$$

where $2\Delta\theta$ is the horizontal angular acceptance, and $2\Delta\phi\sin\theta \equiv 2\Delta\phi^{\rm v}$ is the vertical angular acceptance. The numerical values of the electron and neutron solid angles are given in Table I for the proposed Q^2 points.

Table I. Acceptances and Solid Angles for Hall A HRS (in normal mode) and $\Delta\theta_e = \pm 1.70° = 29.7$ mr, $x = 2.54$ m, $\Delta\theta_n = \pm 5.7° = \pm 50$ mr, and $\Delta\phi_n^{\rm v} = h/2x = \pm 100$ mr

Q^2	E	$\pm\Delta\phi_e^{\rm v}$	$\Delta\Omega_e$	$\pm\Delta\theta_{dev}$	$\pm\Delta\phi_n$	$\Delta\Omega_n$
$(\mathrm{GeV}/c)^2$	(GeV)	(mr)	(msr)	(deg)	(mr)	(msr)
0.6	3.2	26.0	3.09	5.3	105.0	21.0
0.8	4.0	24.3	2.89	4.6	106.0	21.2
1.0	4.0	27.8	3.30	4.1	108.0	21.6
1.2	4.0	31.0	3.68	3.7	112.0	22.4

4.3.3 An Effect of Finite Neutron Momentum in the C.M.

Equation (1) is the result of integration over the final nucleon solid angle; however, when $E_{np}^{c.m.} \neq 0$, the vector p_n^{lab} lies within a cone with an opening angle (*i.e.*, the angle between the neutron and proton momenta) defined by

$$\tan\Delta\theta_{dev} = p_n^{c.m.}/k^{lab} \quad , \tag{19}$$

Values for $\Delta\theta_{dev}$ are listed in Table I for $E_{np}^{c.m.} = 1.5$ MeV (the middle point of the 0–3 MeV bin). For this value of $E_{np}^{c.m.}$, the nucleon motion in the *c.m.* results in an angular spread $\Delta\theta_{dev}$ in the laboratory from $\pm$ 5.3° to $\pm$ 3.1° for the considered Q^2 range. We choose the dimensions of the analyzing detectors in the polarimeter and the flight path to fit this condition because then the integration over 4π in the *c.m.* is justified for the neutrons. For $x = 2.54$ m, $\Delta\theta_n = \pm 5.7°$ and we detect all neutrons from the considered reaction and do not care about their momenta. The corresponding values are listed in Table I.

5 Flight Path and Energy Resolution

In this experiment, the horizontal angular acceptance of the electron arm cannot exceed $\Delta\theta_e = \pm 1.70°$ with the Hall A high-resolution spectrometer (HRS) in the normal operating mode. The

flight path x (to the center of the analyzer detector) that corresponds to a horizontal angular interval $\Delta\theta_n$ = 29.7 mr for the front neutron detector width w = 10 in = 0.254 m is 4.28 m:

$$x = \frac{w}{2\Delta\theta_n} = \frac{0.254 \text{ m}}{2 \times 29.7 \text{ mr}} = 4.28 \text{ m} \tag{20}$$

At this flight path and for a resolving time τ = 0.70 ns (fwhm), neutron energy resolutions are listed in Table II for the proposed points at Q^2 between 0.6 and 1.6 (GeV/c)^2. The neutron energy resolution are calculated from the usual relation:

$$\frac{\Delta T}{T} = \gamma(\gamma+1)\left[\left(\frac{\Delta t}{t}\right)^2 + \left(\frac{\Delta x}{x}\right)^2\right]^{1/2} . \tag{21}$$

Table II. Neutron Energy Resolution*

Q^2	T_n	γ	t	$\Delta T/T$	ΔT
(GeV/c)^2	(MeV)	$(1-\beta^2)^{-1/2}$	(ns)	(%)	(MeV)
0.6	80	1.085	21.8	5.7	4.6
0.8	107	1.114	19.2	6.3	6.8
1.0	133	1.142	17.5	6.9	9.1
1.2	160	1.170	16.3	7.4	11.8

* For x = 2.54 m, $\Delta x = \pm$ 5.0 cm, and $\Delta t = \pm$ 0.35 ns.

6 Counting Rate and Beam Time Estimates

Counting rate estimates for forward electron scattering are made for four Q^2 values of 0.6, 0.8, 1.0, and 1.2 (GeV/c)^2; in this Q^2 interval, the theory with the Buck–Gross wave function[13] predicts a change of sign and a rapid increase of the polarization.

In threshold kinematics, the electron beam energy and Q^2 determine unambiguously the neutron emission angle (Table III) because $\mathbf{p}^{lab} = \mathbf{k}^{lab}/2$ if $E_{np}^{c.m.} = 0$, where $\mathbf{p}_n^{lab} \equiv \vec{p}_n$ is the three–momentum of the neutron in the lab system; however, for $E_{np}^{c.m.} = 1.5$ MeV, the neutron c.m. momentum $|\mathbf{p}^{\text{c.m.}}| = 37$ MeV/c and the neutron emission angle in the lab system with respect to $\mathbf{k}^{lab}$ can reach, *e.g.*, 3.7 deg at $Q^2 = 1.2$ (GeV/c)^2. In the estimates, we believe that all outgoing neutrons in the considered kinematic range are detected by the polarimeter at angles determined by electron kinematics. In these estimates, we approximated the average value of the cross section in the range $E_{np}^{c.m.}$ = 0–3 MeV by the corresponding cross section value at $E_{np}^{c.m.} = 1.5$ MeV.

To do this experiment, we need high momentum resolution (10^{-4}) in the electron arm in order to separate the threshold region from the peak of elastic e–d scattering. This resolution requirement will be provided by high–resolution spectrometer (HRS) in Hall A [17].

The kinematic conditions for the proposed experiment are shown in Table III. The model predictions for cross sections and the components of the recoil neutron polarization are given in Table IV at E = 4 GeV (and 3.2 GeV for the point $Q^2 = 0.6$ (GeV/c)^2). Estimated counting rates are listed in Table V. Also presented in Table V are values for the normal polarization component P_y,

the neutron kinetic energy T_n in the lab system, and the beam time needed to measure P_y. The estimates have shown that P_y measurements with the uncertainties specified in Table V within the range Q^2 = 0.6–1.2 (GeV/c)^2, $E_{np}^{c.m.}$ = 0–3 MeV and 0.2 (GeV/c)^2 steps in Q^2 will require approximately 983 hours of data acquisition time with a liquid–deuterium target and a total time of 1610 hours as detailed in Section 7. The projected results are shown in Fig. 3 for the Buck–Gross wavefunction.

Table III. Kinematic Conditions

Q^2	E	θ_e	E'	θ_n	T_n	$\|\mathbf{p}\|^{lab} = \vec{p}_n$
$(\mathrm{GeV}/c)^2$	(GeV)	(deg)	(GeV)	(deg)	(MeV)	(MeV/c)
0.6	3.2	14.3	3.04	72.5	80	396
0.8	4.0	13.2	3.78	69.9	107	460
1.0	4.0	14.9	3.73	67.6	133	518
1.2	4.0	16.4	3.68	65.5	160	571

Table IV. Values of the Neutron Polarization Components

Q^2	E	$d^2\sigma/d\Omega_e dp_e$	$d^2\sigma/d\Omega_e dE_{np}^{c.m.}$			
$(\mathrm{GeV}/c)^2$	(GeV)	(pb/sr · MeV)	(pb/sr · MeV)	P_x	P_y	P_z
0.6	3.2	91.8	87.4	−0.018	0.106	0.018
0.8	4.0	25.2	23.9	−0.002	0.070	0.007
1.0	4.0	5.69	5.32	0.003	−0.050	0.000
1.2	4.0	1.45	1.34	−0.003	−0.18	−0.003

Table V. Counting Rates and Data Acquisition Times to Measure P_y with a Statistical Accuracy ΔP_y

Q^2	P_y	T_n	Rate	ΔP_y	10^4 N	Beam Time
$(\mathrm{GeV}/c)^2$	___	(MeV)	R (events/min)	___	(events)	T (hours)
0.6	0.106	80	11.5	0.025	2.0	29
0.8	0.070	107	2.95	0.025	2.0	113
1.0	−0.050	133	0.75	0.025	2.0	444
1.2	−0.18	160	0.21	0.050	0.50	397
					Total	983

7 Beam Time Request

The beam time request is as follows:

Activity		Beam on Target (Hours)
1. Tuneup and checkout		60
1.1 Electron spectrometer	24	
1.2 Neutron polarimeter	24	
1.3 Electron–neutron coincidences	12	
2. Data acquisition		1283
2.1 LD_2 target	983	
2.2 Dummy target cell	100	
2.3 Shadow shield (with LD_2 target)	100	
2.4 LH_2 target	100	
3. Overhead (10%)		134
4. Contingency ($\sim$ 10%)		133
		1610

References

[1] M. Bernheim *et al.*, Phys. Rev. Lett. **46**, 402 (1981); S. Auffret *et al.*, *ibid.* **55**, 1362 (1985).

[2] R. G. Arnold *et al.*, SLAC Report No. SLAC-PUB-4918, 1989; M. B. Frodyma, Ph.D.Thesis, University of Massachusetts (1990).

[3] K. S. Lee *et al.*, Phys. Rev. Lett. **67**, 2634 (1991).

[4] B. Sommer, Nucl. Phys. **A308**, 263 (1978); J. F. Mathiot, *ibid.* **A412**, 201 (1984); W. Leidemann, H. Arenhövel, *ibid.* **A393**, 385 (1983); A. Buchmann *et al.*, *ibid.* **A443**, 726 (1985); D. O. Riska, Phys. Scr. **31**, 107 (1985).

[5] E. Truhlik and K. S. Schmitt, Few-Body Systems **11**, 155 (1992).

[6] T. S. Cheng, L. S. Kisslinger, Nucl. Phys. **A457**, 602 (1986); Y. Yamauchi *et al.*, *ibid.* **A443**, 628 (1985); L. Ya. Glozman *et al.*, Phys. Lett. **B200**, 406 (1988).

[7] J. Jourdan *et al.*, CEBAF Proposal PR-89-047 (1989).

[8] A. V. Afanasev, M. P. Rekalo, Acta. Phys. Pol. **B19**, 727 (1988).

[9] A. V. Afanasev, M. P. Rekalo, Preprint ICTP No. IC/91/325, Miramare-Trieste (1991).

[10] M. P. Rekalo *et al.*, J. Phys. G: Nucl. Phys. **15**, 1223 (1989).

[11] M. P. Rekalo, Ukr. Fiz. Zh. **31**, 805 (1986) (In Russian).

[12] M. P. Rekalo *et al.*, J. Phys. G: Nucl. Phys. **13**, 1209 (1987).

[13] W. Buck, F. Gross, Phys. Rev. **D20**, 2361 (1979).

[14] R. G. Arnold et al., Phys.Rev. **C21**, 1426 (1980).

[15] R. Madey *et al.*, IEEE Trans. on Nucl. Sci. **36**, 231 (1989) and private communication.

[16] T. Eden *et al.*, Bates Linear Accelerator Center Annual Scientific and Technical Report 1989, 48–60 (1990).

[17] CEBAF Conceptual Design Report (1990).

[18] M. Lacombe *et al.*, Phys. Lett. **101B**, 139 (1981).

Table Captions

Table I. Acceptances and Solid Angles

Table II. Neutron Energy Resolutions

Table III. Kinematics for the proposed experiment (E = 4 GeV, $E_{np}^{c.m.}$ = 1.5 MeV). The neutron emission angle θ_n and energy T_n are given by the relation $\mathbf{p}_{ls} = \mathbf{k}_{ls}/2$, where $\mathbf{k}_{ls}$ is the three-momentum of the neutron in the lab system. The point Q^2 = 0.6 (GeV/c)^2 is measured with E = 3.2 GeV to keep θ_e larger than the minimal angle of HRS (12.5°).

Table IV. Model predictions for the cross section and neutron polarization (for $E_{np}^{c.m.}$ = 1.5 MeV and for the Buck–Gross deuteron wavefunction with $\lambda = 0.6$).

Table V. Counting rates and beam time needed to measure the normal component of the neutron polarization P_y. Luminosity $L = 3.0 \times 10^{38}$ cm^{-2}s^{-1}, $E_{np}^{c.m.}$ = 0–3 MeV, a radiative correction factor of 0.8, and a neutron transmission factor of 0.38. The number of events needed to achieve this accuracy is given by $N = (1+2/r)/(A_y \Delta P_y)^2$. For the neutron polarimeter figure-of-merit, we used the value $A_y^2 \varepsilon_p = (0.40)^2(0.25 \times 10^{-2}) = 4.0 \times 10^{-4}$ [15], and for the ratio of the real counting rate R to the accidental counting rate A, $r = 2$ was used.

Figure Captions

Fig. 1 The differential cross section of $d(e,e')pn$ vs. Q^2 at $E_{np}^{c.m.}$ = 1.5 MeV and Θ_e = 155° for different deuteron wave functions: Paris [18] (dash-dotted curve) and Buck–Gross [13] with λ = 0, 0.6, 1 (dashed, solid, and dotted curves, respectively). The experimental data are from ref.[1] (diamonds) for $E_{np}^{c.m.}$ = 0–3 MeV and ref.[2] (squares) for $E_{np}^{c.m.}$ = 0–10 MeV.

Fig. 2 The same as in Fig. 1 but with all multipoles set to zero except for the $M1 \rightarrow {}^1S_0$ amplitude. In this case, the diffractive minimum can be seen clearly.

Fig. 3 Normal component of the neutron polarization vector vs. Q^2 in the threshold $d(e,e'\vec{n})p$ ($E_{np}^{c.m.}$ = 1.5 MeV, E = 4 GeV). The notation is the same as in Fig. 1.

Fig. 4 A schematic diagram of the experimental arrangement.

Fig. 5 Neutron polarimeter.

Fig. 6 A plan view of the steel collimator and shielding enclosure housing the neutron polarimeter for CEBAF E89–05.

Fig. 7 A side view of the steel collimator and shielding enclosure housing the neutron polarimeter for CEBAF E89–05.

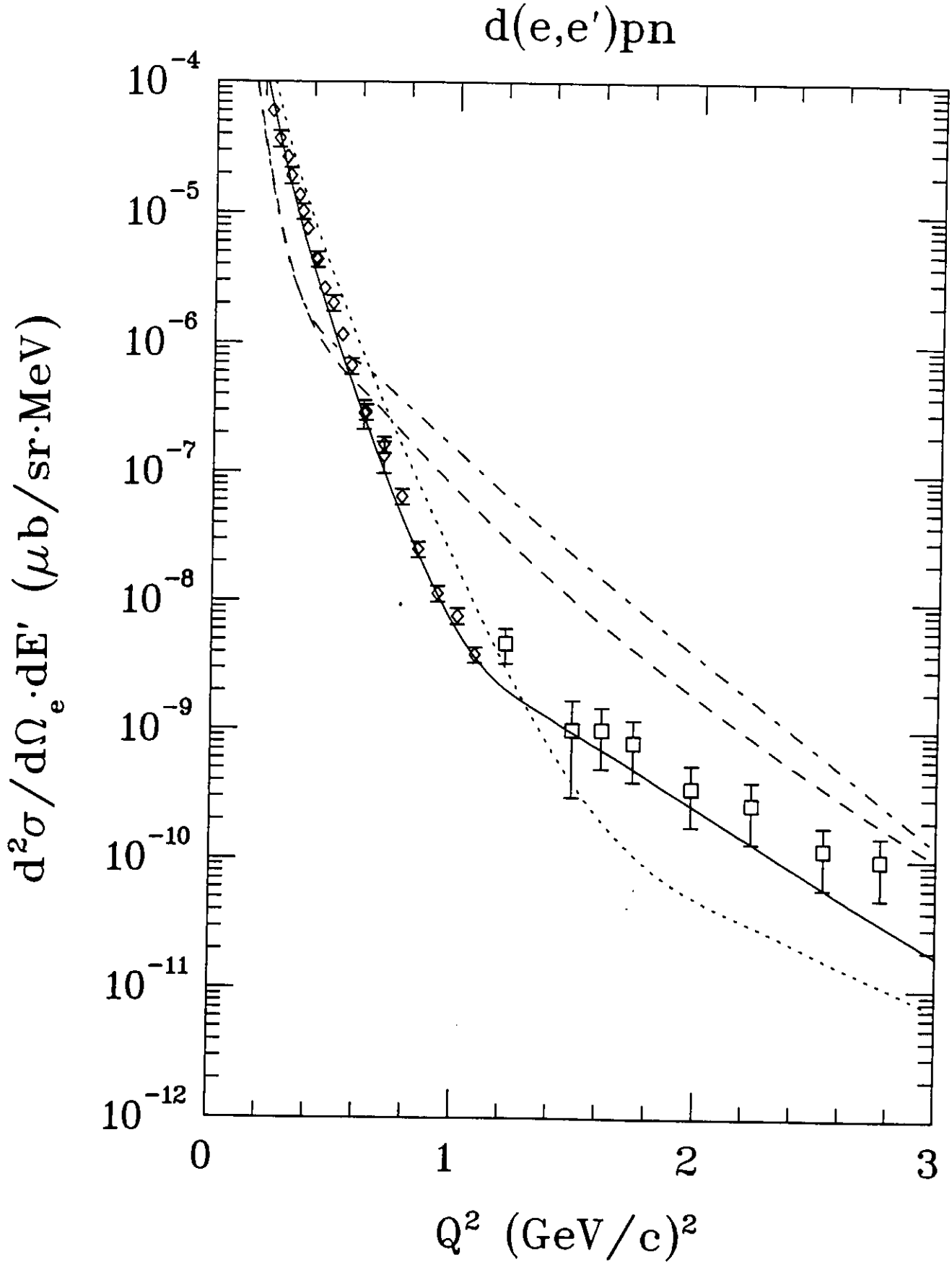
d(e,e′)pn
$d^2\sigma/d\Omega_e \cdot dE'$ (μb/sr·MeV)
10^{-4}
10^{-5}
10^{-6}
10^{-7}
10^{-8}
10^{-9}
10^{-10}
10^{-11}
10^{-12}
0
1
2
3
Q^2 (GeV/c)^2

Fig. 1

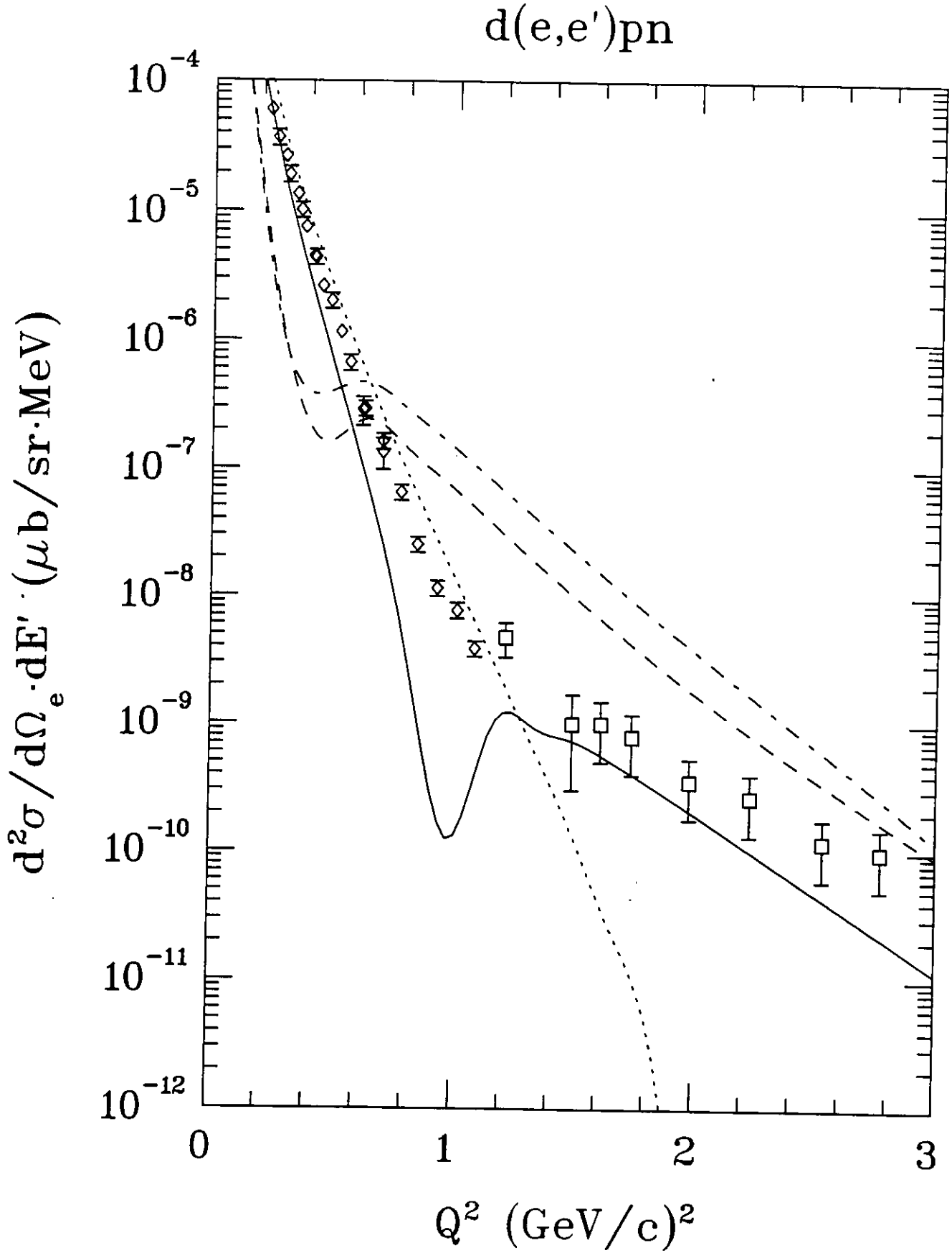
d(e,e')pn
10^{-4}
10^{-5}
10^{-6}
10^{-7}
10^{-8}
10^{-9}
10^{-10}
10^{-11}
10^{-12}
$d^2\sigma/d\Omega_e \cdot dE' \cdot (\mu b/sr \cdot MeV)$
0
1
2
3
Q^2 (GeV/c)^2

Fig. 2

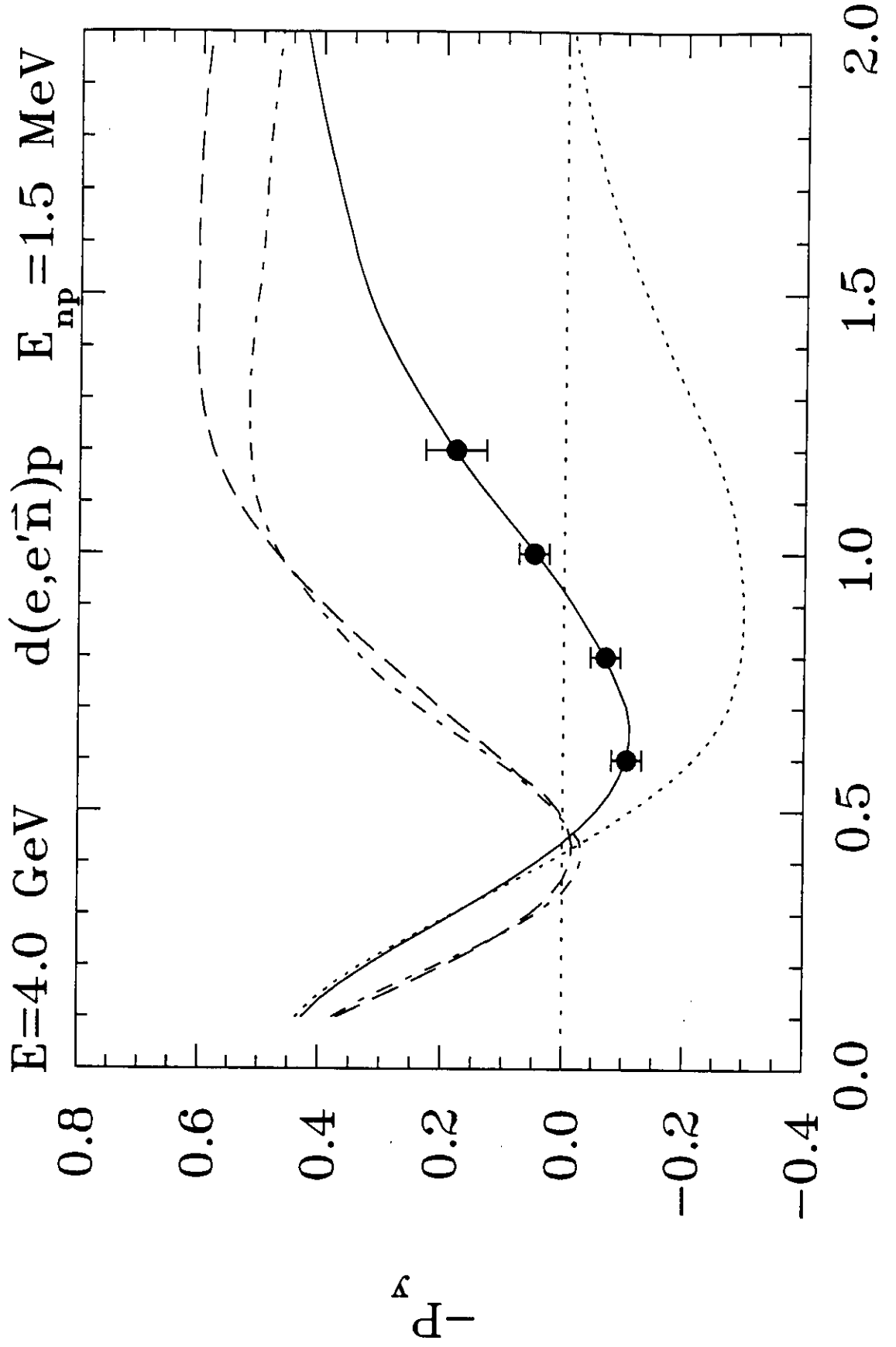
E=4.0 GeV
d(e,e'n⃗)p
E_np =1.5 MeV
−P_y
Q² (GeV/c)²
0.8
0.6
0.4
0.2
0.0
−0.2
−0.4
0.0
0.5
1.0
1.5
2.0

Fig. 3

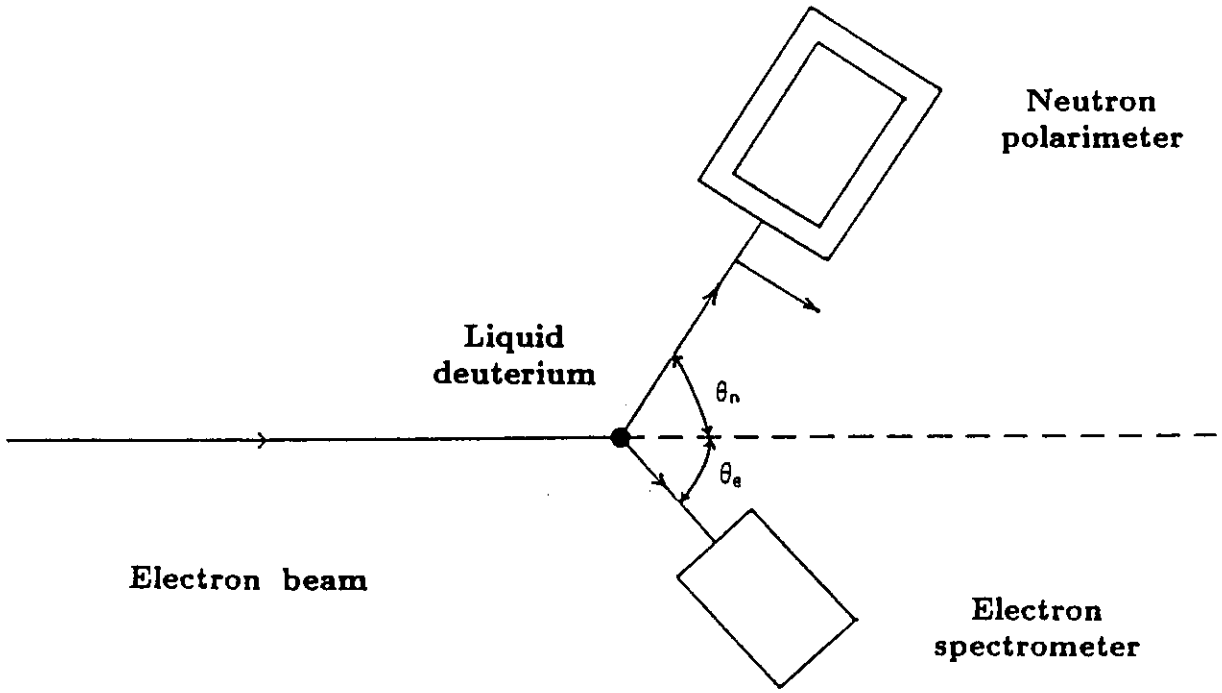
Neutron
polarimeter
Liquid
deuterium
θ_n
θ_e
Electron beam
Electron
spectrometer

Fig. 4

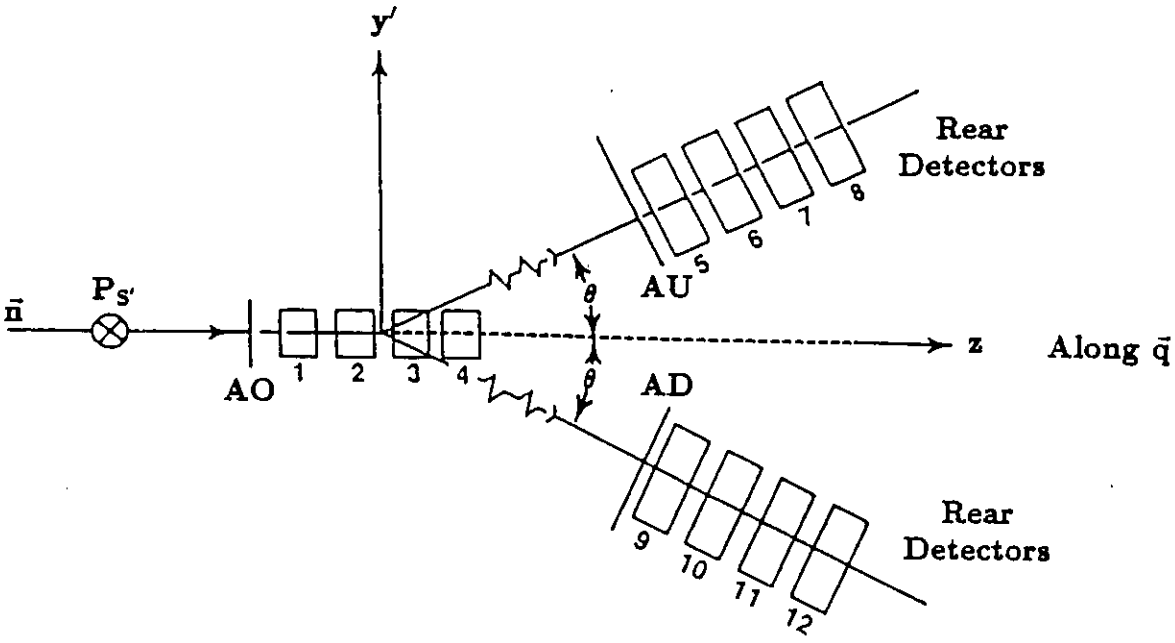
y'
Rear
Detectors
AU
5
6
7
8
$\vec{n}$
$P_{S'}$
θ
z
Along $\vec{q}$
AO
1
2
3
4
θ
AD
Rear
Detectors
9
10
11
12

Fig. 5

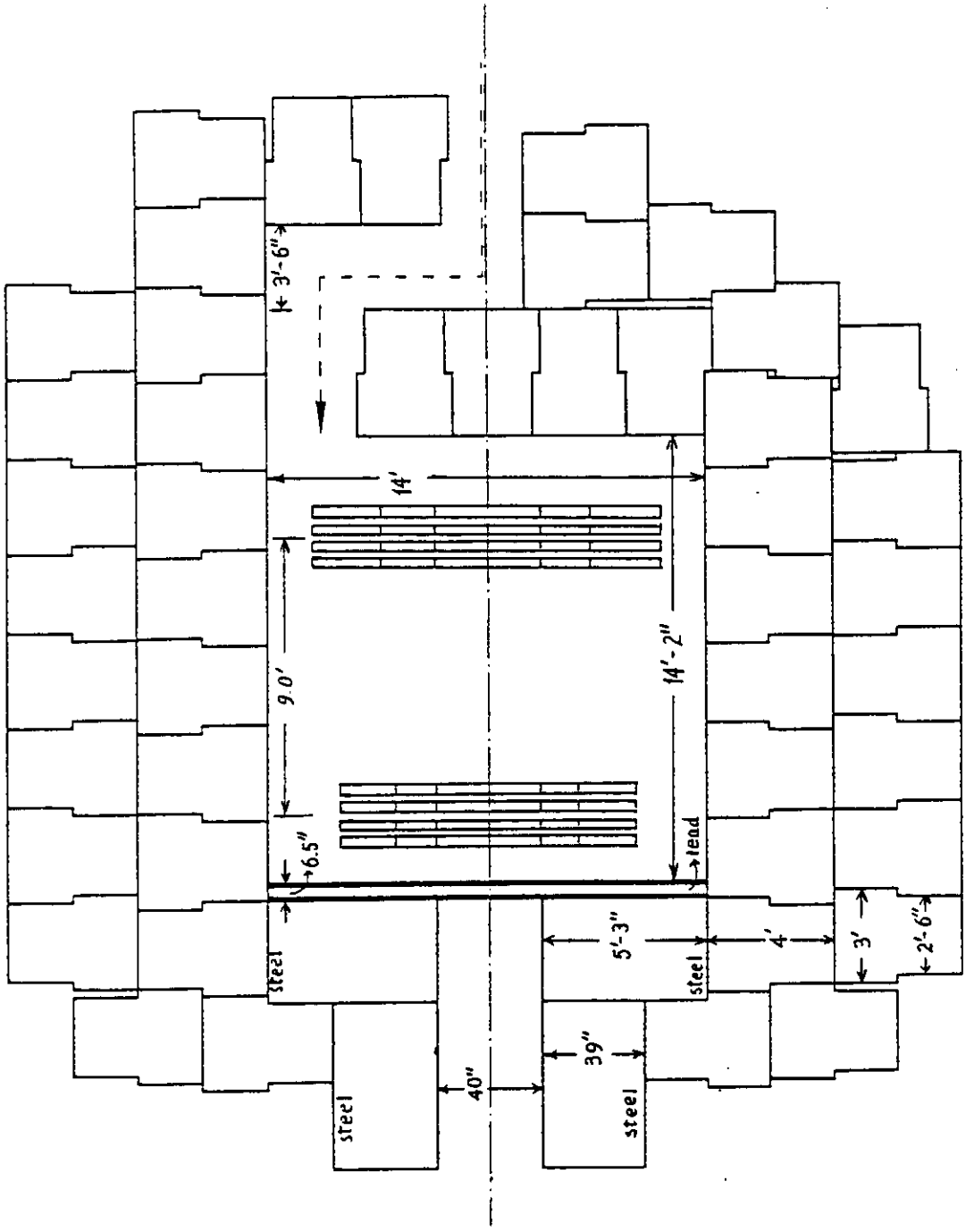

Fig. 6

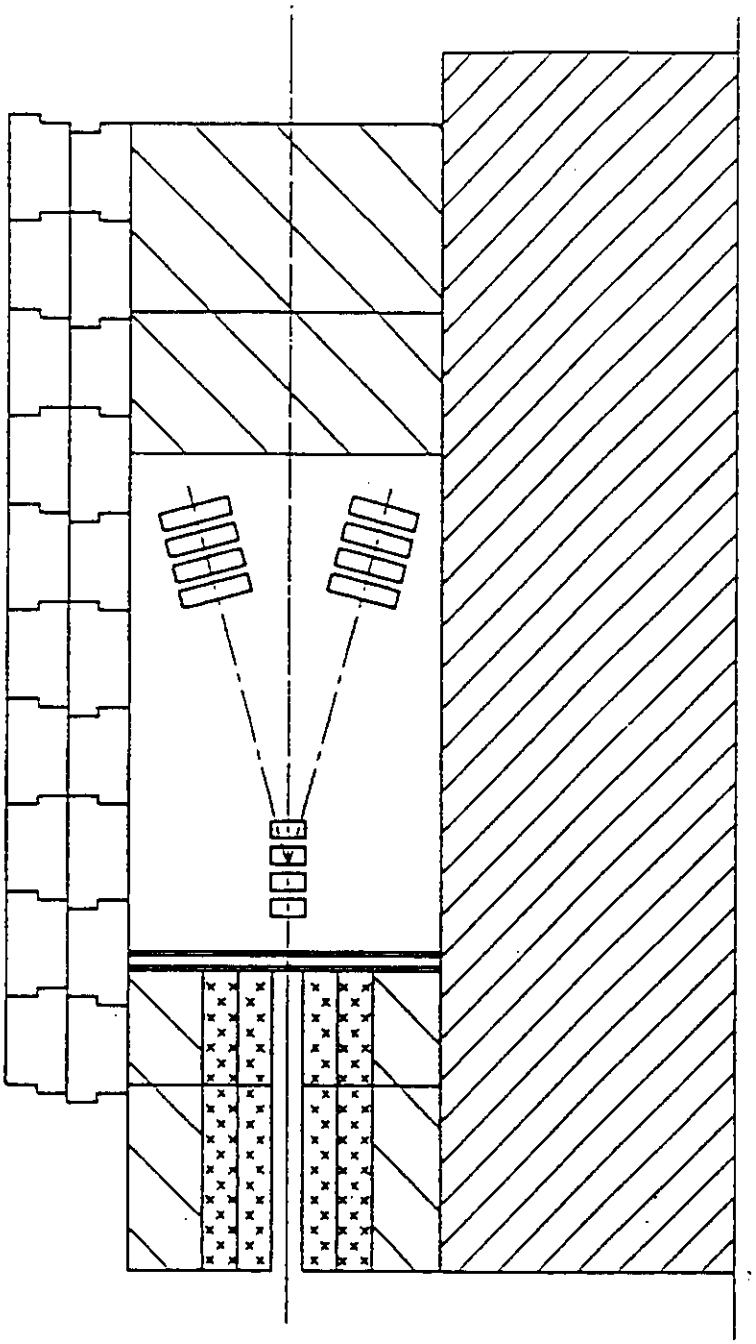

Fig. 7